Long-Lived Inverse Chirp Signals from Core-Collapse in Massive Scalar-Tensor Gravity

Ulrich Sperhake,[1,2,*] Christopher J. Moore,[1,3] Roxana Rosca,[1] Michalis Agathos,[1] Davide Gerosa,[2] and Christian D. Ott[2]

[1]*DAMTP, Centre for Mathematical Sciences, University of Cambridge, Wilberforce Road, Cambridge CB3 0WA, United Kingdom*
[2]*TAPIR 350-17, Caltech, 1200 East California Boulevard, Pasadena, California 91125, USA*
[3]*IST-CENTRA, Departamento de Física, Avenida Rovisco Pais 1, 1049 Lisboa, Portugal*

This Letter considers stellar core collapse in massive scalar-tensor theories of gravity. The presence of a mass term for the scalar field allows for dramatic increases in the radiated gravitational wave signal. There are several potential *smoking gun* signatures of a departure from general relativity associated with this process. These signatures could show up within existing LIGO-Virgo searches.

Introduction.—General relativity (GR) has successfully passed numerous tests [1,2] and, in the words of Ref. [3], "occupies a well-earned place next to the standard model as one of the two pillars of modern physics." And yet, the enigmatic nature of *dark energy* and *dark matter* evoked in the explanation of cosmological and astrophysical observations [4], as well as theoretical considerations regarding the renormalization of the theory in a quantum theory sense, indicates that GR may ultimately need modifications in the low- and/or high-energy regime [5].

Tests of GR have so far been almost exclusively limited to relatively weak fields. But the recent breakthrough detection of gravitational waves (GWs) by LIGO [6] has opened a new observational channel towards strong-field gravity, and tests of Einstein's theory are a key goal of the new field of GW physics [7,8]. Most GW-based tests either (i) construct a phenomenological parameterization of possible deviations from the expected physics and seek to constrain the different parameters or (ii) model the physical system in the framework of a chosen alternative theory to see if it can better explain the observed data.

The latter approach faces significant challenges; the candidate theory must agree with GR in the well-tested weak-field regime and yet lead to measurable strong-gravity effects. Furthermore, a mathematical understanding of the theory, in particular, its well-posedness, is necessary for fully nonlinear simulations. One of the most popular candidate extensions of GR are scalar tensor (ST) theories of gravity [9,10], adding a scalar sector to the vector and tensor fields of Maxwell GR. Scalar fields naturally arise in higher-dimensional theories including string theory and feature prominently in cosmology, and ST theories have a well-posed Cauchy formulation. ST theories also give rise to the most concrete example of a strong deviation from GR known to date: the *spontaneous scalarization* of neutron stars [11]. The magnitude of this effect facilitates strong constraints on the parameter space of the ST theory through binary pulsar observations [12–14]. These bounds, as well as the impressive constraints obtained from the Cassini mission [15], however, are all based on observations of widely separated

objects and, therefore, apply only to the massless ST theory [or theories with a scalar mass $\mu \lesssim 10^{-19}$ eV yielding a Compton wavelength, $\lambda_c = (2\pi\hbar)/(\mu c)$, greater than or comparable to the objects' separation [3,16]].

Deviations of black-hole spacetimes from GR are limited in ST gravity due to the *no-hair* theorems [17,18], although we note that scalar radiation has been observed in black-hole binary simulations for nontrivial scalar potentials [19] or boundary conditions [20]. Nevertheless, the most straightforward way to bypass the no-hair theorems is to depart from the vacuum. Neutron stars and stellar core collapse thus appear to be the most promising systems to search for characteristic signatures; cf. [21–23], and references therein.

Here, we perform the first study of dynamic strong-field systems in *massive* ST theory through exploring GW generation in core collapse. As we will see below, the GW signal is dominated by the rapid phase transition from weak to strong scalarization and the ensuing dispersion of the signal. We therefore focus in this study on spherically symmetric models which capture the key features of the collapse responsible for spontaneous scalarization.

The most promising range of the scalar field mass μ for generating strong scalarization and satisfying existing binary pulsar constraints has been identified as $\mu \gtrsim 10^{-15}$ eV [16,24]. In massive ST theory, low-frequency modes with $f < f_* = \mu/(2\pi\hbar)$ decay exponentially with distance rather than radiate towards infinity. For masses $\mu > 10^{-13}$ eV ($f_* > 24.2$ Hz), the GW power detectable inside the LIGO sensitivity window 10 Hz $\lesssim f \lesssim 10^3$ Hz would be considerably reduced due to this effect. We therefore study in this work the range 10^{-15} eV $\lesssim \mu \lesssim 10^{-13}$ eV.

Formalism.—The starting point of our formulation is the generic action for a scalar-tensor theory of gravity that (i) involves a single scalar field nonminimally coupled to the metric, (ii) obeys the covariance principle, (iii) results in field equations of at most second differential order, and (iv) satisfies the weak equivalence principle. In the Einstein frame, the action can be written in the form (using natural units $G = c = 1$) [5,10]

$$S = \int dx^4 \frac{\sqrt{-\bar{g}}}{16\pi}[\bar{R} - 2\bar{g}^{\mu\nu}\partial_\mu\varphi\partial_\nu\varphi - 4V(\varphi)] + S_m, \quad (1)$$

where φ is the scalar field, $V(\varphi)$ the potential, and $\bar{R}$ and $\bar{g}$ the Ricci scalar and determinant constructed from the conformal metric $\bar{g}_{\mu\nu}$, respectively. S_m denotes the contribution due to matter fields, that couple to the physical or Jordan-Fierz metric $g_{\mu\nu} = \bar{g}_{\mu\nu}/F(\varphi)$, $F(\varphi)$ the coupling function, and the physical energy momentum tensor is $T^{\mu\nu} = 2(-g)^{-1/2}\delta S_m/\delta g_{\mu\nu}$, assumed here to describe a perfect fluid with baryon density ρ, pressure P, internal energy ϵ, enthalpy H, and 4-velocity u^α:

$$T_{\alpha\beta} = \rho H u_\alpha u_\beta + P g_{\alpha\beta}, \qquad H = 1 + \epsilon + P/\rho. \quad (2)$$

The equations of motion are given by

$$\bar{G}_{\alpha\beta} = 2\partial_\alpha\varphi\partial_\beta\varphi - \bar{g}_{\alpha\beta}\partial^\mu\varphi\partial_\mu\varphi + 8\pi\bar{T}_{\alpha\beta} - 2V\bar{g}_{\alpha\beta},$$

$$\bar{\nabla}^\mu\bar{\nabla}_\mu\varphi = 2\pi(F_{,\varphi}/F)\bar{T} + V_{,\varphi},$$

$$\bar{\nabla}_\mu\bar{T}^{\mu\alpha} = -\frac{1}{2}\frac{F_{,\varphi}}{F}\bar{T}\bar{g}^{\alpha\mu}\partial_\mu\varphi, \qquad \nabla_\mu(\rho u^\mu) = 0, \quad (3)$$

where the conformal energy momentum tensor is $\bar{T}_{\alpha\beta} = T_{\alpha\beta}/F$, $\bar{\nabla}$ is the covariant derivative constructed from $\bar{g}_{\mu\nu}$, the subscript $,\varphi$ denotes $d/d\varphi$, and the last equation arises from conservation of the matter current density in the physical frame.

Henceforth, we assume spherical symmetry, writing

$$d\bar{s}^2 = \bar{g}_{\mu\nu}dx^\mu dx^\nu = -F\alpha^2 dt^2 + FX^2 dr^2 + r^2 d\Omega^2, \quad (4)$$

where $\alpha = \alpha(t, r)$, $X = X(t, r)$, and we also define for convenience $\Phi = \ln(\sqrt{F}\alpha)$ and the gravitational mass $m = r[1 - (FX^2)^{-1}]/2$. In spherical symmetry, the 4-velocity in the Jordan frame is $u^\mu = (1 - v^2)^{-1/2}[\alpha^{-1}, vX^{-1}, 0, 0]$, where the velocity field v as well as the other matter variables ρ, P, ϵ, and H are also functions of (t, r). High-resolution shock capturing requires a flux conservative formulation of the matter equations which is achieved by (cf. [23]) changing from variables (ρ, v, H) to

$$D = \frac{\rho X F^{-3/2}}{\sqrt{1 - v^2}}, \qquad S^r = \frac{\rho H v F^{-2}}{(1 - v^2)}, \qquad \tau = \frac{S^r}{v} - \frac{P}{F^2} - D. \quad (5)$$

Finally, we introduce $\eta = X^{-1}\partial_r\varphi$ and $\psi = \alpha^{-1}\partial_t\varphi$. The resulting system of equations is identical to Eqs. (2.21), (2.22), (2.27), (2.28), and (2.33)–(2.39) in Ref. [23] except for the following additional potential terms (bracketed numbers denote right-hand sides in Ref. [23]):

$$\partial_r\Phi = [2.21] - rFX^2 V,$$

$$\partial_r m = [2.22] + r^2 V,$$

$$\partial_t\psi = [2.28] - \alpha F V_{,\varphi},$$

$$s_{S^r} = [2.38] - rV\alpha XF(S^r v - \tau - D + F^{-2}P), \quad (6)$$

where s_{S^r} is the source term in the evolution of S^r. All other equations in the above list remain unaltered.

We have implemented these equations by adding the potential terms to the GR1D code originally developed in Ref. [25] and extended to the massless ST theory in Ref. [23]. As in Ref. [23], we use a phenomenological hybrid equation of state (EOS) $P = P_c + P_{th}$, $\epsilon = \epsilon_c + \epsilon_{th}$ with the *cold* part

$$\rho \leq \rho_{nuc}: \quad P_c = K_1\rho^{\Gamma_1}, \qquad \epsilon_c = \frac{K_1}{\Gamma_1 - 1}\rho^{\Gamma_1 - 1},$$

$$\rho > \rho_{nuc}: \quad P_c = K_2\rho^{\Gamma_2}, \qquad \epsilon_c = \frac{K_2}{\Gamma_2 - 1}\rho^{\Gamma_2 - 1} + E_3, \quad (7)$$

where $\rho_{nuc} = 2 \times 10^{14}$ g cm^{-3}, $K_1 = 4.9345 \times 10^{14}$ [cgs], and K_2 and E_3 follow from continuity; ϵ_{th} measures the departure of the evolved internal energy ϵ from the cold contribution and generates a thermal pressure component $P_{th} = (\Gamma_{th} - 1)\rho\epsilon_{th}$. We thus have three parameters to specify the EOS. As in Ref. [23], we consider $\Gamma_1 = \{1.28, 1.3, 1.32\}$ for the subnuclear, $\Gamma_2 = \{2.5, 3\}$ for the supernuclear EOS, and $\Gamma_{th} = \{1.35, 1.5\}$ for the thermal part describing a mixture of relativistic and non-relativistic gases. For the conformal factor, we use the quadratic Taylor expansion commonly employed in the literature [11,26], and the potential endows the scalar field with a mass μ:

$$F = \exp(-2\alpha_0\varphi - \beta_0\varphi^2), \qquad V = \hbar^{-2}\mu^2\varphi^2/2. \quad (8)$$

The discretization, grid, and boundary treatment are identical to those described in detail in Sec. 3 of Ref. [23].

Simulations.—For the simulations reported here, we employ a uniform grid with $\Delta r = 166$ m inside $r = 40$ km and logarithmically increasing grid spacing up to the outer boundary at 9×10^5 km. As detailed in Supplemental Material [27], we observe convergence between first and second order, in agreement with the use of first- and second-order accurate discretization techniques in the code, resulting in a numerical uncertainty of about 4% in the wave signals reported below.

All simulations start with the WH12 model of the catalog of realistic pre-SN models [28] with initially vanishing scalar field. The evolution is then characterized by six parameters: the above-mentioned EOS parameters Γ_1, Γ_2, and Γ_{th} as well as the mass μ of the scalar field and α_0, β_0 in the conformal function which we vary in the ranges $0 \leq \mu \leq 10^{-13}$ eV, $10^{-4} \leq \alpha_0 \leq 1$, and $-25 \leq \beta_0 \leq -5$. Our observations in these simulations are summarized as follows. (i) The collapse dynamics are similar to the scenario displayed in the left panels in Fig. 4 in Ref. [23]. As conjectured therein, the baryonic matter strongly affects the scalar radiation but itself is less sensitive to the scalar field. (ii) For sufficiently negative β_0, the scalar field reaches amplitudes of the order of unity, independent of the EOS. Even in the massless case $\mu = 0$, we observe this strong scalarization; the key impact of the

massive field therefore lies in the weaker constraints on α_0, β_0 rather than a direct effect of terms involving μ. For illustration, we plot in Fig. 1 the wave signal $r\varphi$ extracted at 5×10^4 km for various parameter combinations. These waveforms are to be compared with those obtained for present observational bounds in the core collapse in massless ST theory as shown in Fig. 6 of Ref. [23]. The amplitudes observed here are larger by $\sim 10^4$ for neutron star formation from less massive progenitors and even exceed the strong signals in black hole formation from more massive progenitors by ~ 100. This *hyperscalarization* of the collapsing stars in massive ST theory (as compared with the more strongly constrained massless case) and the resulting substantially larger GW signals are one of the key results of this work. Translating this increase into improved observational signatures for GW detectors, however, requires the careful consideration of the signal's dispersion as it propagates from the source to the detector; this is the subject of the remainder of this Letter.

Wave extraction and propagation.—At large distances from the source, the dynamics of the scalar field are well approximated by the flat-space equation $\partial_t^2 \varphi - \nabla^2 \varphi + \hbar^{-2} \mu^2 \varphi = 0$, which, in spherical symmetry, reduces to a 1D wave equation for $\sigma \equiv r\varphi$. Plane-wave solutions propagate with group and phase velocities $v_{g/p} = [1 - (\omega_*^2/\omega^2)]^{\pm 1/2}$ for angular frequencies above $\omega_* \equiv \mu/\hbar$ but are exponentially damped for lower frequencies.

In the massless case ($\mu = 0$), the general solution for σ is the sum of an ingoing and an outgoing pulse propagating at the speed of light. This makes interpreting the output of core collapse simulations particularly simple; one extracts the scalar field $\sigma(t; r_{\rm ex})$ at a sufficiently large *extraction radius* $r_{\rm ex}$, and after imposing outgoing boundary conditions the signal at $r > r_{\rm ex}$ is $\sigma(t; r) = \sigma(t - (r - r_{\rm ex}); r_{\rm ex})$.

In the massive case, the situation is complicated by the dispersive nature of wave propagation. However, an analytic solution for the field at large radii can still be written down,
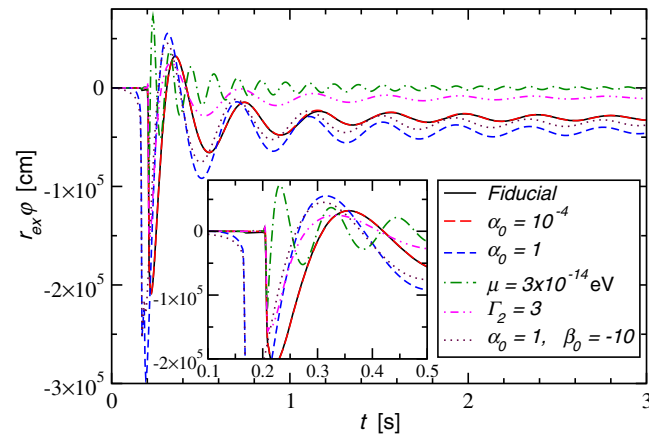

FIG. 1. Waveforms extracted at 5×10^4 km. The legend lists deviations from the fiducial parameters $\mu = 10^{-14}$ eV, $\alpha_0 = 10^{-2}$, $\beta_0 = -20$, $\Gamma_1 = 1.3$, $\Gamma_2 = 2.5$, and $\Gamma_{\rm th} = 1.35$.

albeit in the frequency domain: $\tilde{\sigma}(\omega; r) \equiv \int dt \sigma(t; r) e^{i\omega t}$. The boundary conditions need to be modified for the massive case; frequencies $|\omega| > \omega_*$ propagate, and we continue to impose the outgoing condition for these; however, frequencies $|\omega| < \omega_*$ are exponential (growing or damped), and we impose that these modes decay with the radius. These conditions determine the Fourier transform of the signal at large radii in terms of the signal on the extraction sphere (note the ω ranges):

$$\tilde{\sigma}(\omega; r) = \tilde{\sigma}(\omega; r_{\rm ex}) \begin{cases} e^{-i\sqrt{\omega^2 - \omega_*^2}(r - r_{\rm ex})} & \text{for } \omega < -\omega_*, \\ e^{+i\sqrt{\omega^2 - \omega_*^2}(r - r_{\rm ex})} & \text{for } \omega > -\omega_*. \end{cases} \quad (9)$$

Note that the power spectrum $|\tilde{\sigma}(\omega; r)|^2$ is unchanged during propagation except for the exponential suppression of frequencies $|\omega| < \omega_*$.

As signals propagate, they spread out in time, but the frequency content above the critical frequency ω_* remains unchanged. Consequently, the number of wave cycles in the signal increases with propagation distance; cf. Fig. 2. In the limit of large distances (relevant for LIGO observations of galactic supernovae), the signals are highly oscillatory; i.e., the phase varies much more rapidly than the frequency, and the inverse Fourier transform of Eq. (9) may be evaluated in the *stationary phase approximation* (SPA) [29]. At each instant, the signal is quasimonochromatic with frequency

$$\Omega(t) = \omega_* / \sqrt{1 - [(r - r_{\rm ex})/t]^2} \quad \text{for } t > r - r_{\rm ex}. \quad (10)$$

This time-frequency structure sounds like an *inverse chirp*, with high frequencies arriving before low ones. The origin of this structure can be understood by noting that each frequency component arrives after the travel time of the associated group velocity. Using the SPA, the time domain signal is given by $\sigma(t, r) = A(t, r) \cos \phi(t, r)$, where

$$\phi(t, r) = \sqrt{\Omega^2 - \omega_*^2}(r - r_{\rm ex}) - \Omega t - \frac{\pi}{4} + \text{Arg}[\tilde{\sigma}(\Omega, r_{\rm ex})],$$

$$A(t, r) = \sqrt{\frac{2}{\pi}} \frac{(\Omega^2 - \omega_*^2)^{3/4}}{\omega_* (r - r_{\rm ex})^{1/2}} \text{Abs}[\tilde{\sigma}(\Omega, r_{\rm ex})], \quad (11)$$

and the SPA frequency $\Omega(t)$ is given by Eq. (10).

The Jordan frame metric perturbation is determined by the scalar field φ (the tensorial GW degrees of freedom vanish in spherical symmetry). Any GW detector, small compared to the GW wavelength $\lambda = 2\pi/\omega$, measures the *electric* components of the Riemann tensor R_{0i0j} [2]. In the massless ST theory, this 3-tensor is transverse to the GW wave vector, $R_{0i0j} \propto \delta_{ij} - k_i k_j$, with strain amplitude $h_B = 2\alpha_0 \varphi$ (this is called a *breathing* mode). In massive ST theory, there is an additional *longitudinal* mode, $R_{0i0j} \propto k_i k_j$, with suppressed amplitude $h_L = (\omega_*/\omega)^2 h_B$. A GW interferometer responds identically (up to a sign) to both of these polarizations, meaning they cannot be distinguished [2]; henceforth, we refer to the overall measurable *scalar* signal with amplitude
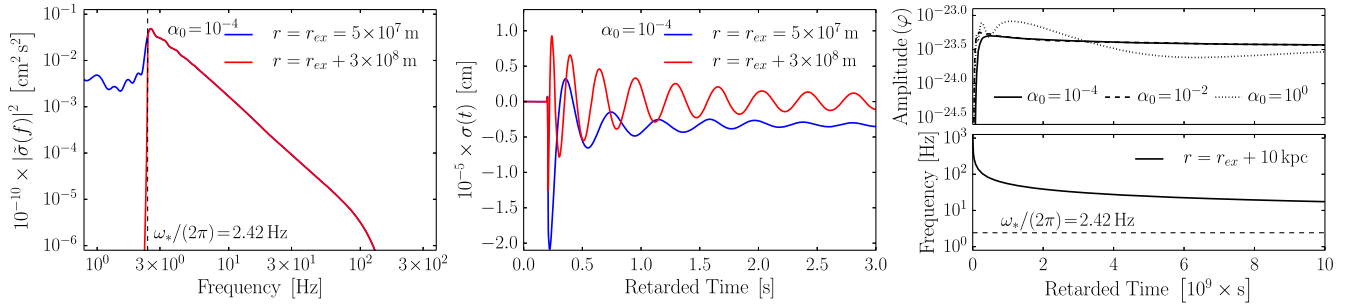
FIG. 2.   Left panel: The frequency-domain power spectrum of the scalar field $\sigma \equiv r\varphi$ at the extraction sphere and 1 light second further out; the exponential decay of frequencies $f < \omega_*/(2\pi)$ can be clearly seen. This simulation was performed for a 12 $M_\odot$ star with $\mu = 10^{-14}$ eV, $\alpha_0 = 10^{-4}$, and $\beta_0 = -20$. Center panel: The time-domain scalar field profiles for the two curves shown in the left panel; during the 1s of propagation, the signal becomes increasingly oscillatory, and the long-lived memory effect is exponentially suppressed. Right panels: The amplitude (top) and frequency (bottom) as functions of time for the scalar field φ from the same simulation as the other panels but at a distance of 10 kpc (it is not practical to plot the long, highly oscillatory time-domain signals at large distances). Also shown by the dotted and dashed curves are the amplitude profiles from other simulations using $\alpha_0 = 10^{-2}$ and $\alpha_0 = 10^0$; the amplitude of the scalar field depends relatively weakly on α_0. For the simulations shown here, the energy radiated in scalar GWs is $\sim 10^{-3}$ $M_\odot$.

$h_S = h_B - h_L = 2\alpha_0[1 - (\omega_*/\omega)^2]\varphi$. In practice, this factor reduces the strain only by at most a few percent at $t \lesssim 10^{10}$ s.

LIGO observations.—GW signals from stellar collapse in ST theory may show up in several ways in existing LIGO-Virgo searches. In each case, there is, in principle, a smoking gun which allows the signal to be distinguished from other types of sources. Here, it is argued that a new dedicated program to search for ST core collapse signals is not needed; however, the results of this work should be kept in mind in analyzing results from existing searches.

Monochromatic searches.—The highly dispersed signal [described by Eq. (11); see right panels in Fig. 2] at large distances can last for many years and is nearly monochromatic on time scales of $\lesssim 1$ month. Quasimonochromatic GWs with slowly evolving frequency may also be generated by rapidly rotating nonaxisymmetric neutron stars; the scalar signals described in this Letter can be distinguished from neutron stars by the scalar polarization content and the highly characteristic frequency evolution described in Eq. (10).

These signals may be detected by existing monochromatic searches and allow for the determination of the scalar mass from the frequency change $\dot{f}$. The signals may show up in *all-sky* searches; however, greater sensitivities can be achieved via *directed* searches at known nearby supernovae (all-sky searches achieved sensitivities that constrain $h \lesssim 9.7 \times 10^{-25}$ [30], whereas model-based, directed searches at a supernova remnant have achieved sensitivities of $h \lesssim 2.3 \times 10^{-25}$ [31] at frequencies ~ 150 Hz). Methods to detect signals of any polarization content have recently been presented in Ref. [32]; note that interferometers are a factor ~ 2 less sensitive to scalar than tensor GWs. A directed search should begin within a few months to years of the supernova observation and may last for decades with sensitivity improving as time$^{-1/2}$ (see the amplitude as a function of time in Fig. 2). In fact, the amplitude can remain at detectable levels for so long that directed searches aimed

at historical nearby supernovae (e.g., SN1987A) may be worthwhile; a nondetection from such a search can place the most stringent constraints to date on certain regions of the massive ST parameter space, (μ, α_0, β_0). [For $\mu = 10^{-14}$ eV, for example, we obtain for SN1987A a frequency $\Omega/(2\pi) \approx 128$ Hz and rate of change $\dot{\Omega}/(2\pi) \approx 2$ Hz/yr, using distance $D := r - r_{ex} = 51.2$ kpc and time $t - D = 30$ yr.]

In any monochromatic search there would be two smoking gun features indicating an origin of hyperscalarized core collapse in the massive ST theory: the scalar polarization content and the long signal duration with gradual frequency evolution according to Eq. (10). Our simulations suggest that the intrinsic amplitude of the scalar field is insensitive to α_0, β_0, and μ over wide parameter ranges. However, the GW strain scales linearly with the coupling; $h \propto \alpha_0\varphi$. Extrapolating the results in Fig. 2 suggests that if a supernova at 10 kpc were to be observed and followed up by a directed monochromatic search by aLIGO at design sensitivity, the coupling could be constrained to $\alpha_0 \lesssim 3 \times 10^{-4}$ (assuming no signal was in fact observed), which compares favorably with the impressive Cassini bound in the massless case [15].

Stochastic searches.—As shown above, stellar core collapse in massive ST theory can generate large amplitude signals, allowing them to be detected at greater distances. However, the signals propagate dispersively, spreading out in time and developing a sharp spectral cutoff at the frequency of the scalar mass. The long duration signals from distant sources can overlap to form a stochastic background of scalar GWs with a characteristic spectral shape around this frequency. A detailed analysis of this stochastic signal covering a wider range of ST parameters and progenitor models will be presented in Ref. [33].

Burst searches.—If the scalar field is light ($\mu \lesssim 10^{-20}$ eV), then signals originating within the galaxy will not be significantly dispersed [e.g., the spread in arrival

times across the LIGO bandwidth, $(10–10^3)$ Hz, for a source at 10 kpc is $\lesssim 1$ s]. These short-duration, burstlike scalar GW signals may be detected using strategies similar to those used to search for standard core collapse super-novae in GR. However, for these light scalar fields the observational constraints on the coupling constants α_0 and β_0 rule out the hyperscalarized signals shown in Fig. 1, and the amplitudes are similar to those reported in Ref. [23].

Discussion.—The main results of our work are the following points. (i) Weaker constraints on the coupling parameters α_0, β_0 in ST theory with scalar masses $\mu \gtrsim 10^{-15}$ eV allow for scalarization in stellar core collapse orders of magnitude above what has been found in massless ST theory. The scalar signature is rather insensitive to the EOS parameters and varies only weakly with the ST parameters α_0 and β_0 for sufficiently negative β_0. (ii) The strong scalar GW signal disperses as it propagates over astrophysical distances, turning it into an inverse chirp signal spread out over years with a near monochromatic signature on time scales of ∼1 month. (iii) We identify three existing GW search strategies (continuous wave, stochastic, and burst searches) that have the capacity to observe these signals for galactic sources or infer unprec-edented bounds on the massive ST theory's parameter space through nondetection.

The dispersion of the signal has two significant conse-quences. (i) While the number of individually observable events may not change significantly from pure GR expect-ations (a few per century, largely in the Milky Way and Magellanic Clouds), each event remains visible for years or even centuries, vastly increasing the number of sources visible *now*. (ii) The signal to be detected is largely insensitive to details of the original source. Instead, it is mainly characterized by the overall magnitude of the scalarization and the ST parameters, most notably the mass μ. We tentatively conjecture that other prominent astrophysi-cal sources, such as a NS binary inspiral and merger, may result in a similar inverse-chirp imprint on the GW signal in the massive ST theory. A natural extension of our work is the exploration of other theories of gravity with massive degrees of freedom (e.g., [34]), but the results reported here already demonstrate the qualitatively new range of opportunities offered in this regard by the dawn of GW astronomy.

*us248@maths.cam.ac.uk

[1] D. Psaltis, Living Rev. Relativity **11**, 9 (2008).
[2] C. M. Will, Living Rev. Relativity **17**, 4 (2014).
[3] J. Alsing, E. Berti, C. M. Will, and H. Zaglauer, Phys. Rev. D **85**, 064041 (2012).
[4] D. N. Spergel, Science **347**, 1100 (2015).
[5] E. Berti *et al.*, Classical Quantum Gravity **32**, 243001 (2015).
[6] B. P. Abbott *et al.*, Phys. Rev. Lett. **116**, 061102 (2016).
[7] B. P. Abbott *et al.*, Phys. Rev. Lett. **116**, 221101 (2016).
[8] N. Yunes, K. Yagi, and F. Pretorius, Phys. Rev. D **94**, 084002 (2016).
[9] T. Damour and G. Esposito-Farése, Classical Quantum Gravity **9**, 2093 (1992).
[10] Y. Fujii and K. Maeda, *The Scalar-Tensor Theory of Gravitation* (Cambridge University Press, Cambridge, England, 2007).
[11] T. Damour and G. Esposito-Farèse, Phys. Rev. Lett. **70**, 2220 (1993).
[12] P. C. C. Freire, N. Wex, G. Esposito-Farèse, J. P. W. Verbiest, M. Bailes, B. A. Jacoby, M. Kramer, I. H. Stairs, J. Antoniadis, and G. H. Janssen, Mon. Not. R. Astron. Soc. **423**, 3328 (2012).
[13] J. Antoniadis *et al.*, Science **340**, 1233232 (2013).
[14] N. Wex, in *Brumberg Festschrift*, edited by S. M. Kopeikin (de Gruyter, Berlin, 2014).
[15] B. Bertotti, L. Iess, and P. Tortora, Nature (London) **425**, 374 (2003).
[16] F. M. Ramazanoğlu and F. Pretorius, Phys. Rev. D **93**, 064005 (2016).
[17] S. W. Hawking, Commun. Math. Phys. **25**, 167 (1972).
[18] K. S. Thorne and J. J. Dykla, Astrophys. J. **166**, L35 (1971).
[19] J. Healy, T. Bode, R. Haas, E. Pazos, P. Laguna, D. M. Shoemaker, and N. Yunes, Classical Quantum Gravity **29**, 232002 (2012).
[20] E. Berti, V. Cardoso, L. Gualtieri, M. Horbatsch, and U. Sperhake, Phys. Rev. D **87**, 124020 (2013).
[21] J. Novak and J. M. Ibáñez, Astrophys. J. **533**, 392 (2000).
[22] C. Palenzuela, E. Barausse, M. Ponce, and L. Lehner, Phys. Rev. D **89**, 044024 (2014).
[23] D. Gerosa, U. Sperhake, and C. D. Ott, Classical Quantum Gravity **33**, 135002 (2016).
[24] S. Morisaki and T. Suyama, Phys. Rev. D **96**, 084026 (2017).
[25] E. O'Connor and C. D. Ott, Classical Quantum Gravity **27**, 114103 (2010).
[26] T. Damour and G. Esposito-Farése, Phys. Rev. D **54**, 1474 (1996).
[27] See Supplemental Material at http://link.aps.org/supplemental/10.1103/PhysRevLett.119.201103 for code tests and a convergence analysis.
[28] S. E. Woosley and A. Heger, Phys. Rep. **442**, 269 (2007).
[29] C. Bender and S. Orszag, *Advanced Mathematical Methods for Scientists and Engineers* (McGraw-Hill, New York, 1978).
[30] B. P. Abbott *et al.*, Phys. Rev. D **94**, 042002 (2016).
[31] B. P. Abbott *et al.*, Astrophys. J. **847**, 47 (2017).
[32] M. Isi, M. Pitkin, and A. J. Weinstein, Phys. Rev. D **96**, 042001 (2017).
[33] C. J. Moore, M. Agathos, U. Sperhake, and R. Rosca (to be published).
[34] F. M. Ramazanoğlu, Phys. Rev. D **96**, 064009 (2017).